# dc-Magnetic-Field Generation in Unmagnetized Shear Flows

T. Grismayer,[1,*] E. P. Alves,[1] R. A. Fonseca,[1,2] and L. O. Silva[1,†]

[1]GoLP/Instituto de Plasmas e Fusão Nuclear—Laboratório Associado, Instituto Superior Técnico, 1049-001 Lisboa, Portugal
[2]DCTI/ISCTE Instituto Universitário de Lisboa, 1649-026 Lisboa, Portugal

(Received 30 October 2012; published 3 July 2013)

The generation of dc magnetic fields in unmagnetized electron-ion shear flows is shown to be associated to either initial thermal effects or the onset of electron-scale shear instabilities, in particular the cold Kelvin-Helmholtz instability. This mechanism, intrinsic to shear gradients on the electron scale, is described through a kinetic model that predicts the growth and the saturation of the dc field in both scenarios. The theoretical results are confirmed by multidimensional particle-in-cell simulations, demonstrating the formation of long-lived magnetic fields ($t \sim 100's\ \omega_{pi}^{-1}$) along the full longitudinal extent of the shear layer, with a typical transverse width of $\sqrt{\gamma_0}c/\omega_{pe}$, reaching magnitudes $eB_{\mathrm{dc}}/m_e c\omega_{pe} \sim \beta_0\sqrt{\gamma_0}$ for an initial sharp shear. The case of an initial smooth shear is also discussed.

DOI: 10.1103/PhysRevLett.111.015005 PACS numbers: 52.38.Kd, 52.35.Mw, 52.35.Tc, 52.38.Dx

It is well-known that plasma instabilities on the electron kinetic scale can efficiently transform plasma kinetic energy into electric and magnetic-field energy, playing a central role in current high-intensity laser-plasma experiments [1–4] and astrophysical scenarios [5,6]. *Ab initio* particle-in-cell simulations (PIC) have demonstrated the generation of subequipartition magnetic fields, i.e., the ratios between the energy density of the field and the kinetic energy density of the flow are close to $10^{-3}$ to $10^{-2}$ [7–10]. Electron plasma instabilities associated to shear flows, such as the cold Kelvin-Helmholtz instability (KHI) [11,12], however, have been largely overlooked and contain a wealth of unexplored physics, namely, the unexpected generation of a strong dc magnetic field along the shear interface. Recent particle-in-cell simulations have demonstrated the emergence of this large-scale dc magnetic field in unmagnetized electron-ion plasmas with velocity shear [12–14] after the onset of the KHI. Yet this dc field is not captured by the two-fluid KHI theory [11,12,15]. Furthermore, recent experiments have reproduced shear flow conditions [1–3] allowing one to probe the development of the KHI, although the self-generated magnetic fields remain to be diagnosed. In the near future, with the advent of more powerful lasers, experiments will be able to probe the self-generated fields of the KHI and their consequences in astrophysical, laser-produced, and even low-temperature plasmas. It is the purpose of this Letter to identify the physical mechanism responsible for the generation of such dc magnetic fields.

We recall the two-dimensional (2D) theoretical model of the unmagnetized KHI [11,12], which is based on the relativistic fluid formalism of plasmas coupled with Maxwell's equations. Without loss of generality, we focus on symmetrically shearing flows (with velocities $\pm v_0\vec{e}_y$ along the $y$ direction and with equal densities $n_0$) with a tangential discontinuity in the $x$ direction. The protons are considered free-streaming, whereas the electron fluid quantities and fields are linearly perturbed, $u = \bar{u}e^{-k_\perp|x|}e^{i(k_\parallel y-\omega t)}$. The unstable modes are stationary [$\mathrm{Re}(\omega) = 0$] surface waves and obey the following dispersion relation

$$\frac{\Gamma}{\omega_{pe}} = \left[\frac{1}{2\gamma_0^3}\left(\sqrt{1+8\frac{k_\parallel^2 v_0^2\gamma_0^3}{\omega_{pe}^2}} - 1 - 2\frac{k_\parallel^2 v_0^2\gamma_0^3}{\omega_{pe}^2}\right)\right]^{1/2}, \quad (1)$$

where $\Gamma$ is the growth rate [$\mathrm{Im}(\omega)$] of the mode with wave number $k_\parallel$, $\omega_{pe} = \sqrt{4\pi n_0 e^2/m_e}$ is the plasma frequency defined in CGS units, $k_\perp^2 = k_\parallel^2 + \omega_{pe}^2/(c^2\gamma_0) - \omega^2/c^2$, and $\gamma_0 = 1/\sqrt{1-\beta_0^2}$ is the Lorentz factor of the shearing flows with $\beta_0 = v_0/c$. After a few $e$-folding times, the system is dominated by the fastest growing mode with $\Gamma_{\max} = \sqrt{1/8}\gamma_0^{-3/2}\omega_{pe}$ and $k_{\parallel\max} = \sqrt{3/8}\gamma_0^{-3/2}\omega_{pe}/v_0$. In the case of an initial smooth shear, the growth rate decreases as the shear gradient length increases; see Ref. [16].

To ascertain these results and to fully explore the KHI, PIC simulations were performed using OSIRIS [17,18]. We simulate shearing slabs of cold ($v_0 \gg v_{\mathrm{th}}$, where $v_{\mathrm{th}}$ is the thermal velocity) unmagnetized electron-proton plasmas with a reduced mass ratio $m_p/m_e = 100$ ($m_e$ and $m_p$ are respectively the electron and the proton mass) and evolve it up to $\omega_{pi}t = 100$ ($\omega_{pi} = \sqrt{m_e/m_p}\omega_{pe}$ is the proton plasma frequency). We present the simulation results of a shear flow with $v_0 = 0.2c$, which is on the order of the flow velocity driven in intense laser-plasma experiments [4]. The shear flow initial condition is set by a velocity field with $+v_0\vec{e}_y$ in the middle half of the simulation box and a symmetric velocity field with $-v_0\vec{e}_y$ in the upper and lower quarters of the box. Initially, the system is charge and current neutral. Periodic boundary conditions are imposed in every direction. The simulation box dimensions are $100 \times 100(c/\omega_{pe})^2$, resolved with 20 cells per electron

 

skin depth ($c/\omega_{pe}$), and a number of 36 particles per cell per species is used. Space and time are respectively normalized to $c/\omega_{pe}$ and $1/\omega_{pe}$.

The growth and the wave number of the most unstable mode are confirmed by 2D simulations [Fig. 1(a1)]. We measure a wavelength of $2c/\omega_{pe}$ and a growth rate of $0.32\omega_{pe}$, in agreement with the theoretical values $\lambda_{\parallel\max} = 2\pi/k_{\parallel\max} = 2.09c/\omega_{pe}$ and $\Gamma_{\max} = 0.33\omega_{pe}$. Interestingly, the growth of a dc ($k_\parallel = 0$) magnetic-field mode is also observed [Figs. (insets) 1(a2) and 1(b2)], which is not predicted by the linear fluid theory [$\Gamma(k_\parallel = 0) = 0$], nor has it been previously identified in magnetohydrodynamics simulations [19–22] and only recently in kinetic simulations [12]. The growth of the dc-magnetic-field mode results from a current imbalance due to between the electron flows across the shear surface, while the proton flows remain almost unperturbed due to their inertia. The orientation of the dc-magnetic-field peak is mostly determined by the proton current structure, i.e., $\vec{\nabla} \times \vec{B}_{\rm dc} \sim \mu_0 e n_0 \vec{v}_0(x)$. The mixing arises due to the deformation of the electron interface between the two flows, which in the linearized fluid calculations is not accounted for and, in zeroth order, remains fixed. Alternatively, we find that the physics describing the formation of a dc mode can be modeled in a one-dimensional (1D) reduced theory where an initial temperature drives the mixing effect. In order to understand the formation of the dc field, we first consider the one-dimensional case. Initially, all the fields are zero, and we assume a plasma with a tangential shear flow in the $x$ direction and an initial temperature such that $v_{\rm th} \ll v_0$. This setting is not in Vlasov equilibrium, and it is clear that the transient thermal expansion of the electrons across the shear surface (ions are assumed to be cold and free streaming) leads to an imbalance of the current neutrality around the shear surface, forming a dc magnetic field in the $z$ direction. The initial corresponding electron distribution function reads $f(x, v_x, v_y, v_z, t=0) = f_0(v_x, v_y - v_0 \mathrm{sgn}(x), v_z)$. Due to the dimensionality of the problem, one verifies that $E_z$, $B_x$, $B_y$ remain zero. The reduced set of equations is therefore Maxwell's equations coupled with the Vlasov equation $\partial_t F + v_x \partial_x F - (e/m_e)(\vec{E} + (\vec{v}/c) \times \vec{B}_z) \cdot \partial_{\vec{v}} F = 0$ where $F(x, v_x, v_y, t) = \int dv_z f(x, v_x, v_y, v_z, t)$. The formal solution of the Vlasov equation is $F(x, v_x, v_y, t) = F_0(x_0, v_{x0}, v_{y0})$, where $x_0$, $v_{x0}$, and $v_{y0}$ denote the position and velocities of an electron at $t = 0$ and $F_0 = \int dv_{z0} f_0$ [23,24]. At early times, if we assume that the induced fields are sufficiently small that we can neglect their effect on the change of momentum of the electrons, the distribution function can be determined along the free streaming orbits of the electrons [25]. For the sake of simplicity, we separate the initial electronic distribution in two parts, $F_0 = F_0^-(x_0 < 0) + F_0^+(x_0 > 0)$. The electron currents read $J_{e,y}^{\pm} \simeq -e \int dv_y v_y \int dv_x F_0^{\pm}(x - v_x t, v_x, v_y \mp v_0)$. For a Maxwellian distribution function, $f_M(v) = e^{-v^2/2v_{\rm th}^2}/\sqrt{2\pi} v_{\rm th}$, we have $F_0^{\pm}(x_0, v_{x0}, v_{y0} \mp v_0) = n_0 f_M(v_{x0}) f_M(v_{y0} \mp v_0)$ and we obtain $J_{e,y}^{\pm} \simeq \mp e n_0 v_0 \times \int_{\mp x/t}^{\infty} dv_x f_M(v_x) \simeq \mp (e v_0 n_0/2) \mathrm{erfc}(\mp x/\sqrt{2} v_{thx} t)$. The total current is given by adding the unperturbed proton currents $J_{p,y} = e n_0 v_0 \mathrm{sgn}(x)$, from which the magnetic field can be integrated by neglecting the displacement current in Ampère's Law

$$B_{\rm dc} \simeq e 4\pi n_0 \beta_0 \sqrt{2} v_{\rm thx} t \left[ \frac{e^{-\xi^2}}{\sqrt{\pi}} - \xi \mathrm{erfc}(\xi) \right], \qquad (2)$$

where $\xi = |x|/\sqrt{2} v_{thx} t$. We thus verify that the dc-magnetic-field width is on the order of $\sqrt{2} v_{thx} t$ and its peak intensity grows linearly in time as $B_{\rm dc}^{\rm peak} = 4\sqrt{2\pi} e n_0 \beta_0 v_{thx} t$ [Fig. 2(a4)]. This derivation is valid as long as the orbits of the electrons do not diverge much from the free streaming orbits, i.e., as long as the electric and magnetic fields that develop self-consistently do not affect the free motion of the particles. However, the electrons will eventually feel the induced magnetic field, which tends to push more electrons across the shear via the $\vec{v}_0 \times \vec{B}_{\rm dc}$ force.

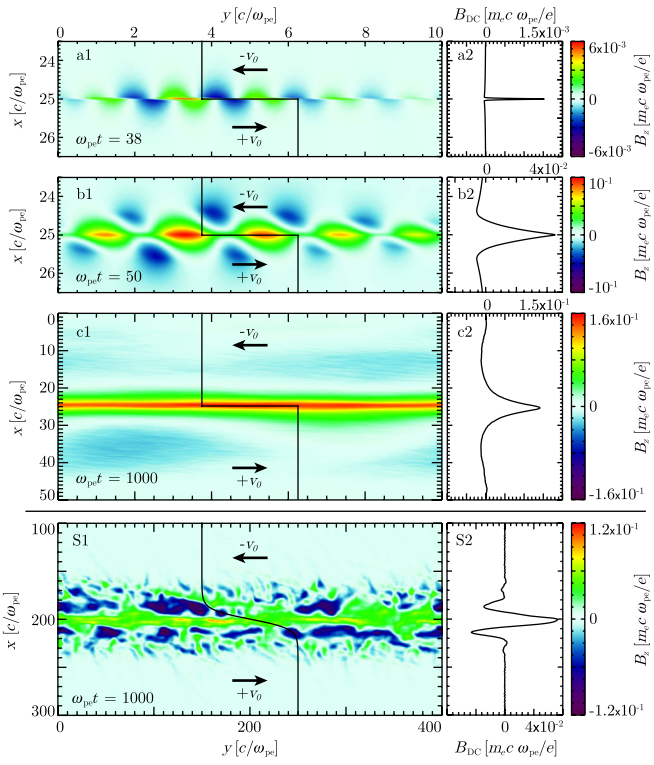


FIG. 1 (color online). $B_z$ component of the magnetic-field structure generated by the cold KHI for $v_0 = 0.2c$ during (a) the linear regime, (b) near saturation, and (c) at $t = 1000\omega_{pe}^{-1} = 100\omega_{pi}^{-1}$. The insets on the right hand side represent the longitudinal average of the magnetic field, revealing the dc component. ($S_1$) and ($S_2$) show the magnetic field at saturation for an initial smooth shear $v_0(x)/c = 0.2 \tanh(x/L)$ with $L = 10c/\omega_{pe} = c/\omega_{pi}$.

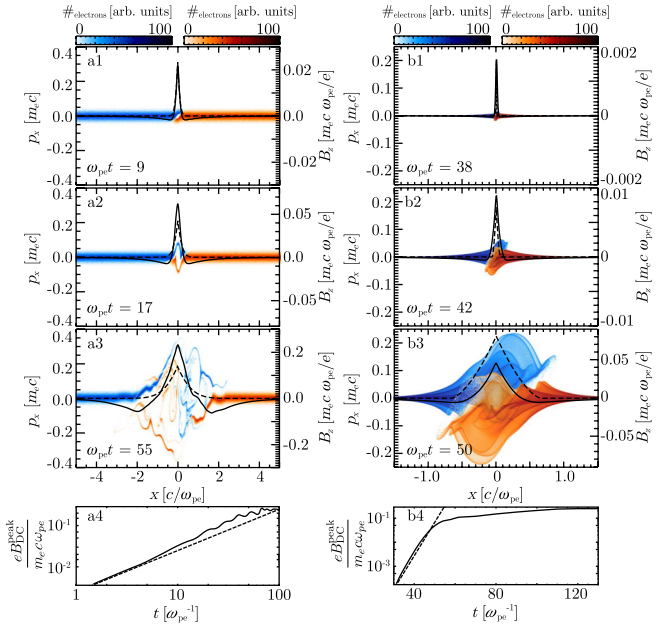


FIG. 2 (color online). Evolution of the electron phase space [(a1)–(a3)] and (b1)–(b3)] and dc-magnetic-field peak [(a4) and (b4)]; log-log scale is used to display linear dc peak evolution in (a4), and log-linear scale is used to display exponential evolution in (b4). Left: 1D warm shear flow with $v_0 = 0.2c$ and $v_{\rm th} = 0.016$. Right: 2D cold shear flow for the same $v_0$. The blue (red) color represents the electrons with a negative (positive) drift velocity $v_0$. The self-consistent dc magnetic field is represented by the solid curve, whereas the dashed curve represents the magnetic field given by the theoretical model. The flow velocity is positive (negative) on the right (left) side of the shear.

Consequently, the rate at which electrons cross the shear increases, which in turn enhances the growth rate of the magnetic field. We find that the displacement current term leads to a $(v_{thx}/c)^2$ correction to the dc-magnetic-field peak at early times (following a simple dimensional analysis of Maxwell's curl equations), which is negligible in our regime. However, the displacement current tends to increase the electron current on either side of the shear interface, eventually building the dc-magnetic-field side wings observed at later times [Figs. 2(a3) and 2(b3)].

In order to verify our analytical calculations and to further investigate the phase where electrons deviate from their free streaming orbits, we carried out 1D simulations of the $x$ direction of the 2D simulations. The Debye length is resolved in the 1D simulations ($\Delta x = \lambda_D$), and we used 1000 particles per cell. Figures 2(a1)–(a3) shows the time evolution of the $xp_x$ phase space and the magnetic field for $v_{\rm th} = 0.016c$ and $v_0 = 0.2c$. At earlier times of $\omega_{pe}t = 9$ [Fig. 2(a1)], an excellent agreement between the model and the simulation is observed. The model breaks down approximately when an electron initially with $v_x = 0$ (around the shear) acquires a velocity change on the order of $v_{thx}$, which corresponds to a strong distortion of the Maxwellian distribution around the shear. Figures 2(a2) and 2(a4) shows this effect at $\omega_{pe}t = 17$. The model underestimates the magnitude of the magnetic field, and one can clearly observe the distortion of the distribution function in the field region. As the magnetic field grows, the Larmor radius ($r_L$) of the electrons crossing the shear interface decreases. When the minimum $r_{\rm L,min}$ (associated to the peak of $B_{\rm dc}$) becomes smaller than the characteristic width of the magnetic field $l_{\rm dc}$, the bulk of the electrons becomes trapped by the magnetic-field structure. This is illustrated in Fig. 2(a3) at $\omega_{pe}t = 55$. The magnetic trapping prevents the electron bulk expansion across the shear (that drives the growth of the magnetic field), saturating the magnetic field. An estimate of the saturation can be obtained by equating $r_{\rm L,min} \sim l_{\rm dc}$. From Eq. (2), it is possible to write the magnetic field as $B_{\rm dc}(x,t) = 4\pi e n_0 \beta_0 w(x,t)$, where $w(0,t)$ should be interpreted as the characteristic width of the field. With $l_{\rm dc} \sim w(0,t)$, $r_{\rm L,min} = \gamma_0 m_e v_0 / eB_{\rm dc}(0,t)$, we find that $l_{\rm dc} \sim c\sqrt{\gamma_0}/\omega_{pe}$, giving the saturation level of the magnetic field as $eB_{\rm dc}^{\rm sat}/m_e c\omega_{pe} \sim \beta_0\sqrt{\gamma_0}$. This scaling has been verified for 1D simulations (Fig. 3).

In the absence of an initial temperature, an alternative mechanism is needed to drive the electron mixing across the shear surface that in turn generates the dc field. This mechanism is the cold fluid KHI that operates in 2D and 3D geometries. In fact, in the warm shear flow scenario, both the cold fluid KHI and the electron thermal expansion can contribute to the generation of the dc field. This happens when the typical length of the dc field due to the thermal expansion ($l_{\rm dc}$) after a few $e$ foldings of the cold fluid KHI ($T_{\rm KHI,growth} = n_{e\text{-foldings}}/\Gamma_{\rm max}$, where $n_{e\text{-foldings}}$ is on the order of 10) is on the order of the relativistic electron skin depth, i.e., $v_{\rm th}T_{\rm KHI,growth} \sim \sqrt{\gamma_0}c/\omega_{pe}$. Therefore, the cold fluid KHI dominates the electron mixing in the limit $v_{\rm th}T_{\rm KHI,growth} \ll \sqrt{\gamma_0}c/\omega_{pe}$.

For a two-dimensional cold plasma undergoing the KHI, the electron distribution function can be

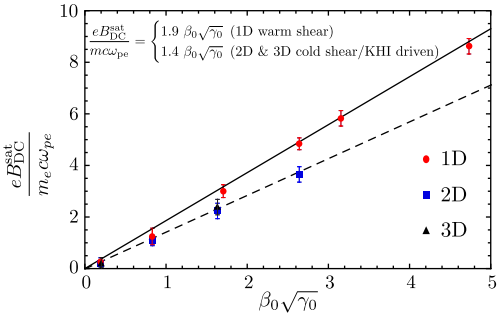


FIG. 3 (color online). Magnitude of the dc-magnetic-field peak at saturation as a function of $\beta_0\sqrt{\gamma_0}$. The red, blue, and black markers represent the results of 1D, 2D, and 3D PIC simulations, respectively. The error bars are associated to the fluctuations of the peak value in the saturation stage. The lines represent best-fit curves to the simulation results, demonstrating the good agreement with the theoretical estimate.

written as $f(x,y,v_x,v_y,v_z,t)=n_0\delta(v_x-v_{x,\mathrm{fl}}(x,y,t))\delta(v_y-v_{y,\mathrm{fl}}(x,y,t))\delta(v_z)$ where $v_{x,\mathrm{fl}}$, $v_{y,\mathrm{fl}}$ correspond to the velocity field solutions of the fluid theory. In this case, the self-generated KHI fields play the role of an effective temperature that transports the electrons across the shear surface, while the protons remain unperturbed, inducing a dc component in the current density and, hence, in the fields. We then have to solve the evolution of the distribution function and show that the current density $J_y$, averaged over a wavelength $\lambda = 2\pi/k_\parallel$, has a nonzero dc part. We follow the same approach as before and calculate the average distribution function defined as $F(x, v_x, t) = (1/\lambda)\int dv_y \int dv_z \int_\lambda dy f(x, y, v_x, v_y, v_z, t)$. To obtain analytical results we will assume that the linearly perturbed fluid quantities are purely monochromatic, which is equivalent to assume that after a few $e$ foldings, the mode corresponding to $k_\parallel = k_{\parallel\max}$ dominates with a growth rate of $\Gamma = \Gamma_{\max}$. We then write $v_{y,\mathrm{fl}} \simeq v_0(x)$ and $v_{x,\mathrm{fl}} = \bar{v}_{x,\mathrm{fl}} \sin(k_\parallel y)e^{-k_\perp|x|+\Gamma t}$, where $\bar{v}_{x,\mathrm{fl}}$ is the amplitude of the velocity perturbations at $t = 0$. We then obtain

$$F(x, v_x, t) = \frac{n_0}{\pi v_{\max}\sqrt{1-\eta^2}}, \tag{3}$$

where $\eta(x,v_x,t)=v_x/v_{\max}(x,t)$ with $v_{\max}(x,t) = \bar{v}_{x,\mathrm{fl}}e^{-k_\perp|x|+\Gamma t}$. We observe that the development of 2D cold KHI [Fig. 2(b)] reveals close similarities with the 1D hot model previously described. In the 2D KHI, averaging the distribution in the direction of the flow shows that the perturbation gives rise to a spread in $v_x$ that may be interpreted as an effective temperature. The spread in $v_x$ decays exponentially away from the shear and grows exponentially with time. The mean velocity is zero, and the effective temperature associated to this distribution function is defined as $V^2_{\mathrm{eff}}(x,t) = (1/n_0)\int dv_x v_x^2 F(x, v_x, t) = v^2_{\max}/2$. One can then expect a similar physical picture as that in the hot shear scenario and, as a result, the emergence of dc components in the fields which are induced by the development of the unstable KH perturbations. The evolution of the phase space in Fig. 2 illustrates the similarity between the warm 1D [Figs. 2(a1)–2(a3)] and cold 2D [Figs. 2(b1)–2(b3)] scenarios.

The challenge in this scenario is to determine how such a distribution function expands across the shear surface due to the complexity of the orbits in the fields structure (multidimensional fields with discontinuities at $x = 0$). In the region where the electron mixing occurs, we assume electron orbits given by $x \sim x_0 + (v_{x0}/\Gamma)e^{\Gamma t}$ and $v_x \sim v_{x0}e^{\Gamma t}$ where $x_0$ and $v_{x0}$ are the position and velocity of a particle at the time $t_0$ when the instability begins. We obtain $J^{\pm}_{e,y}(x,t) \simeq \mp e v_0 \int_{\mp x\Gamma}^{v^0_{\max}} dv_x F(x, v_x, t) \simeq e v_0 n_0[(1/2) \pm (1/\pi)\arcsin(x\Gamma/v^0_{\max})]$ where $x\Gamma \in [-v^0_{\max}, v^0_{\max}]$ and $v^0_{\max}(t) = v_{\max}(x = 0, t)$ that represents the maximum velocity of a particle that was originally in the vicinity of the shear. The limits of the integral represent the deformation of the boundary between the two flows on a characteristic distance of $v^0_{\max}/\Gamma$ as the instability develops. We then find the total current density by summing the proton contribution and integrate to obtain the induced dc magnetic field

$$B_{\mathrm{dc}}(x \gtrless 0, t) = \mp 8 e n_0 \beta_0 x\left[\arcsin(\zeta) \mp \frac{\pi}{2} \pm \sqrt{\frac{1}{\zeta^2}-1}\right] \tag{4}$$

with $\zeta = \Gamma x/v^0_{\max}$. The peak of the dc magnetic field is located at $x = 0$ where the expression above reduces to $B_{\mathrm{dc}}(0, t) = 8e\beta_0 n_0 v^0_{\max}(t)/\Gamma$ and thus grows at the same rate as the KHI fields that can be verified in Fig. 2(b4). One can verify in Figs. 2(b1) and 2(b2) that Eq. (4) shows reasonable agreement with the 2D simulations. This derivation neglects the dc Lorentz force on the electron trajectories, which makes this model valid as long as the induced dc field remains small compared to the fluid fields associated to the mode $k_{\parallel\max}$. The peak of the $B_{\mathrm{dc}}$ field is proportional to $v^0_{\max}(t)$. We therefore conclude that the induced dc magnetic field is always of the same order of the fluid fields [Figs. 1(a) and 1(b)]; thus, its consequences to KHI development cannot be neglected. As the dc field evolves, electrons start to get trapped and we expect a level of saturation similar to the one obtained in the 1D model which is verified by the simulations. The comparisons between the saturation level of the 1D, 2D, and 3D simulations are shown in Fig. 3, verifying the $\beta_0\sqrt{\gamma_0}$ scaling. When a smooth shear is considered, the electron KH still develops, and we verified that the initial electron transport across the shear, due to the development of the instability, is the mechanism triggering magnetic-field generation, therefore validating the physics captured by our model. At saturation, the dc magnetic field has a typical width on the order of the initial shear gradient length and reaches a maximum value of $B_{\mathrm{dc}}(L) \sim B_{\mathrm{dc}}(0)/L$ where $L$ is the initial shear gradient length measured in $c/\omega_{pe}$. Interestingly, the dc magnetic field remains stable beyond the electron time scale and persists up to 100's $\omega_{pi}^{-1}$ as shown in Figs. 1(c) and 1(S). Eventually the protons will drift away from the shear surface due to the magnetic pressure, broadening the dc-magnetic-field structure and lowering its magnitude.

In conclusion, we have shown that the emergence of dc magnetic field is an intrinsic phenomenon associated to electron-ion shear flows. The dc field is generated through the formation of dc current driven by the expansion of electrons in the shear region due to a thermal expansion or the development of the cold fluid KHI perturbations. We have presented an analytical description of the formation of the dc field in agreement with 1D, 2D, and 3D PIC simulations. The dc-magnetic-field saturation on the electron time scale is independent of the type of the expansion and persists up to proton time scales, reaching maximum magnitudes of $eB_{\mathrm{dc}}/mc\omega_{pe} \simeq 1.4\beta_0\sqrt{\gamma_0}$ with thicknesses

of a few $\sqrt{\gamma_0}c/\omega_{pe}$ and, thus, is dynamically relevant for the evolution of the KHI on ion time scales. The effect of an initial smooth shear tends to lower the saturation value proportionally to the initial shear gradient length whereas the thickness increases proportionally.

T. Grismayer and E. P. Alves contributed equally to this work. This work was supported by the European Research Council (ERC-2010-AdG Grant No. 267841) and FCT (Portugal) Grants No. SFRH/BD/75558/2010, No. SFRH/BPD/75462/2010, and No. PTDC/FIS/111720/2009. We acknowledge PRACE for providing access to resource SuperMUC based in Germany at the Leibniz research center. Simulations were performed at the IST cluster (Lisbon, Portugal), and SuperMUC (Germany).

*thomas.grismayer@ist.utl.pt
†luis.silva@ist.utl.pt

[1] E. C. Harding, J. Hansen, O. Hurricane, R. Drake, H. Robey, C. Kuranz, B. Remington, M. Bono, M. Grosskopf, and R. Gillespie, Phys. Rev. Lett. **103**, 045005 (2009).
[2] Y. Kuramitsu *et al.*, Phys. Rev. Lett. **108**, 195004 (2012).
[3] O. A. Hurricane *et al.*, Phys. Rev. Lett. **109**, 155004 (2012).
[4] F. Fiuza, R. A. Fonseca, J. Tonge, W. B. Mori, and L. O. Silva, Phys. Rev. Lett. **108**, 235004 (2012).
[5] M. V. Medvedev and A. Loeb, Astrophys. J. **526**, 697 (1999).
[6] A. Gruzinov and E. Waxman, Astrophys. J. **511**, 852 (1999).
[7] L. O. Silva, R. A. Fonseca, J. W. Tonge, J. M. Dawson, W. B. Mori, and M. V. Medvedev, Astrophys. J. **596**, L121 (2003).
[8] A. Spitkovsky, Astrophys. J. **682**, L5 (2008).
[9] J. T. Frederiksen, C. B. Hededal, T. Haugbølle, and Å. Nordlund, Astrophys. J. **608**, L13 (2004).
[10] H. Karimabadi, V. Roytershteyn, M. Wan, W. H. Matthaeus, W. Daughton *et al.*, Phys. Plasmas **20**, 012303 (2013).
[11] A. Gruzinov, arXiv:0803.1182.
[12] E. P. Alves, T. Grismayer, S. F. Martins, F. Fiúza, R. A. Fonseca, and L. O. Silva, Astrophys. J. **746**, L14 (2012).
[13] M. Hayashi and J. I. Sakai, ITC Research Papers and Research Notes (2004), Vol. 1, pp. 69–72.
[14] M. Boettcher, E. P. Liang, I. A. Smith, and P. Roustazadeh, AIP Conf. Proc. **1505**, 618 (2012).
[15] N. D'Angelo, Phys. Fluids **8**, 1748 (1965).
[16] E. P. Alves, T. Grismayer, S. F. Martins, F. Fiúza, R. A. Fonseca, and L. O. Silva (to be published).
[17] R. A. Fonseca *et al.*, Lect. Notes Comput. Sci. **2331**, 342 (2002).
[18] R. A. Fonseca, S. F. Martins, L. O. Silva, J. W. Tonge, F. S. Tsung, and W. B. Mori, Plasma Phys. Controlled Fusion **50**, 124034 (2008).
[19] W. Zhang, A. MacFadyen, and P. Wang, Astrophys. J. **692**, L40 (2009).
[20] A. Frank, T. W. Jones, D. S. Ryu and J. B. Gaalaas, Astrophys. J. **460**, 777 (1996).
[21] L. Chen and A. Hasegawa, J. Geophys. Res. **79**, 1024 (1974).
[22] X. Zhu and M. G. Kivelson, J. Geophys. Res. **93**, 8602 (1988).
[23] T. M. O'Neil, Phys. Fluids **8**, 2255 (1965).
[24] G. J. Morales and T. M. O'Neil, Phys. Rev. Lett. **28**, 709 (1972).
[25] T. Grismayer, J. E. Fahlen, V. K. Decyk, and W. B. Mori, Plasma Phys. Controlled Fusion **53**, 074011 (2011).